Relation of regional cross-fiber shortening to wall thickening in the intact heart. Three-dimensional strain analysis by NMR tagging

FE Rademakers, WJ Rogers, WH Guier, GM Hutchins, CO Siu, ML Weisfeldt, JL Weiss and EP Shapiro

Circulation 1994;89;1174-1182
Circulation is published by the American Heart Association. 7272 Greenville Avenue, Dallas, TX 72514
 Print ISSN: 0009-7322. Online ISSN: 1524-4539

Relation of Regional Cross-Fiber Shortening to Wall Thickening in the Intact Heart

Three-dimensional Strain Analysis by NMR Tagging

Frank E. Rademakers, MD, PhD; Walter J. Rogers, MS; William H. Guier, PhD; Grover M. Hutchins, MD; Cynthia O. Siu, PhD; Myron L. Weisfeldt, MD; James L. Weiss, MD; Edward P. Shapiro, MD

Background The mechanism by which small amounts of myofiber shortening lead to extensive wall thickening is unknown. When isolated fibers shorten, they thicken in the two orthogonal directions. In situ fibers, however, vary in their orientation through the wall, and each is tethered to near or distant neighbors, which allows shortening to occur both in the direction of the fibers and also perpendicular to them. This "cross-fiber" shortening may enable the wall to shorten in two directions and thereby thicken extensively in the third.

Methods and Results Nuclear magnetic resonance tagging is a noninvasive method of labeling and tracking myocardium of the entire heart in three dimensions that does not interfere with myocardial motion. To investigate the presence and importance of cross-fiber shortening in the intact left ventricle, 10 closed-chest dogs were studied by nuclear magnetic resonance tagging. Five short-axis and four long-axis images were acquired to reconstruct 32 cubes of myocardium in each dog at end diastole and end systole. Pathological dissection was performed to determine the fiber direction at the epicardium, midwall, and endocardium of each cube. Strain was computed from the three-dimensional cube coordinates in the fiber and cross-fiber directions for epicardial and endocardial surfaces, and thickening of the full wall and its epicardial and endocardial halves was determined. Shear deformations were also calculated. Fiber strain at the epicardium and endocardium was $-6.4\pm0.7\%$ and $-8.5\pm0.6\%$ (mean±SEM), respectively (difference, $P>.05$). Cross-fiber strain at epicardium and endocardium was $-0.6\pm0.5\%$ and $-25\pm0.6\%$, respectively (difference, $P<.05$). Thickening of the full wall reached $32.5\pm1.0\%$, composed of epicardial thickening of $25.5\pm0.6\%$ and endocardial thickening of $43.3\pm1.0\%$ (difference, $P<.05$). Fiber/cross-fiber shear strain was small (<3%). Significant regional differences were present in all strains. A significant correlation was found between the extents of regional thickening and cross-fiber shortening.

Conclusions Cross-fiber shortening at the endocardium, therefore, far exceeds cross-fiber shortening at the epicardium and fiber shortening at both epicardium and endocardium. Since no active shortening can occur locally in the cross-fiber direction, the extensive endocardial cross-fiber shortening must result from interaction with differently aligned fibers at a distance. The correlation between regional thickening and cross-fiber shortening supports the hypothesis that this interaction is the mechanism for amplifying small amounts of fiber shortening to cause extensive endocardial thickening. (***Circulation.*** **1994;89:1174-1182.**)

Key Words • ventricles • magnetic resonance imaging • epicardium • endocardium

The mammalian left ventricle (LV) is a highly efficient pump, providing a variable output of 5 to 25 L/min. This pump is built of individual muscle fibers that shorten and thicken during systole as their fundamental repeating unit, the sarcomere, exerts force and shortens along the long axis of the fiber.[1] The magnitude of sarcomere shortening generally does not exceed about 15%.[2] Simple geometric considerations would suggest that this degree of shortening of a cylindrical fiber would result in thickening of about 8%; however, thickening of the LV wall may reach 40% or higher. This discrepancy is also evident from the studies of contraction of the isolated papillary muscle, a long-standing model of myocardial contractile tissue, which also shortens only about 15%.[3] A possible explanation for this disparity can be found in differences in structural morphology: the papillary muscle consists of parallel, longitudinally disposed fibers, whereas the fibers in the intact LV wall change from an oblique orientation at the epicardium to a circumferential orientation at the midwall to a reverse oblique direction at the endocardium.[4-6] This nonparallel disposition permits the interaction of fibers at different depths within the wall and could result in structural rearrangement by which shortening occurs not only along the long axis of the fiber but also perpendicular to it.[7-12] By measuring the deformation of three columns of radiopaque beads implanted at approximately 2-mm intervals through the anterior free wall, Waldman et al[9] demonstrated that such "cross-fiber shortening" is possible and in fact occurs extensively in the inner layers of the LV wall. Those investigators hypothesized that marked shortening in the cross-fiber direction would result in extensive wall thickening, as structural rearrangement allows all mass to be directed into the radial direction.

Since there is considerable region-to-region heterogeneity in LV fiber orientation[6] and LV shortening,[13,14] this hypothesis could be tested by defining the relation between cross-fiber shortening and thickening across

Received August 11, 1993; revision accepted December 4, 1993.

From the Division of Cardiology, The Johns Hopkins University School of Medicine and the Francis Scott Key Medical Center, Baltimore, Md.

Correspondence to Edward P. Shapiro, Division of Cardiology, Francis Scott Key Medical Center, 4940 Eastern Ave, Baltimore, MD 21224.

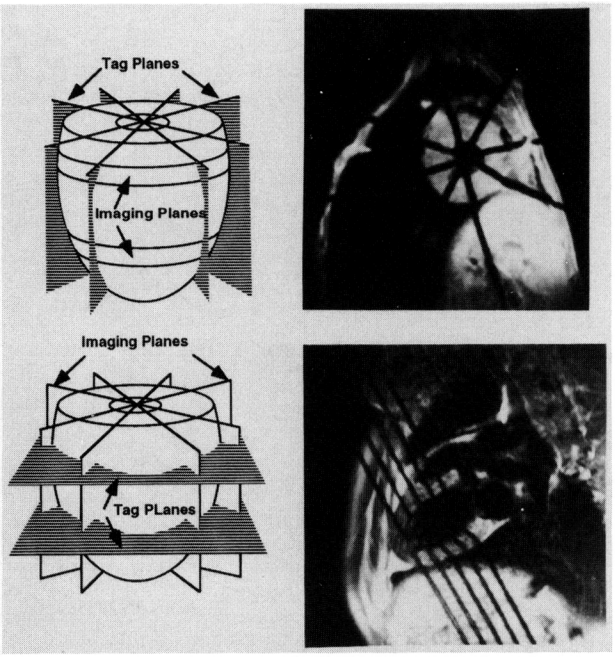

FIG 1. Diagrams showing orientation of tagging and imaging planes with respect to the left ventricle (left) and example of one short-axis (upper right) and one long-axis (lower right) tagged magnetic resonance image.

regions of the LV. However, methods that depend on implantation of beads or devices into the LV wall cannot sample multiple LV sites. In addition, the closely spaced beads used in previous investigations could interfere with myocardial deformation.[15] Magnetic resonance (MR) imaging (MRI) combined with MR tagging[16,17] now provides a unique nondestructive means to mark the myocardium and to measure the strains in the entire LV wall.[13,18] In this study we used MRI with tagging to quantify strain in the fiber direction, in the cross-fiber direction, and in the radial direction. Our goal was to assess the importance of cross-fiber shortening for thickening by defining the interrelations between the strains. We also sought to determine the magnitude of the fiber and cross-fiber strains in the epicardium and endocardium and their regional variability by use of a completely noninvasive method.

Methods

MRI Tissue Tagging

MRI tags are nondestructive markers that appear on images as black lines (Fig 1). They are imprinted on the myocardium at end diastole by selective radiofrequency saturation of planes perpendicular to the imaging planes; they change the magnetization of the protons in the tagged plane compared with the neighboring nontagged regions, resulting in a difference in signal intensity. This difference persists for a time period dependent on the longitudinal relaxation time of myocardium, about 400 to 500 milliseconds for the magnetic field strength used in this study. The value of the tags is that they move with the myocardium throughout the cycle. Thus, tags can track specific locations in much the same manner as implanted radiopaque beads and record changes in position, shape, or orientation of the imprinted myocardium. Tags radial to short-axis images or parallel tags can be generated (Fig 1).

Data Acquisition

General

All images were acquired on a 0.38-T Resonex iron-core resistive magnet system with a spin-echo sequence modified to include tagging, a flexible solenoidal belt coil, a slice thickness of 10 mm, a 25.6-cm field of view, 128 phase and 256 frequency encoding steps, and averaging two excitations. The repetition time was twice the RR interval and the time to echo was 30 milliseconds.

Location of Image Planes

After a series of scout images was obtained, planes orthogonal to the axes of the heart were defined. Five parallel short-axis planes encompassed the ventricle from base to apex. Perpendicular to these, four long-axis planes were positioned to correspond to a four-chamber, a two-chamber, and two intermediate views. In one imaging sequence the short-axis planes were used as imaging planes and the long-axis planes as tagging planes, and in a second sequence this was reversed. On the short-axis image, eight radial tags were therefore visible, and the long-axis images contained 10 parallel tags (Fig 1).

Timing of Image Acquisition

Tags and images were triggered by every other R wave of the ECG. Tags were placed immediately after the trigger. The first image was acquired 60 milliseconds after the first R wave after the tags. With a multislice sequence, images were acquired at 80-millisecond intervals for a total of five time points, extending into the next RR interval (so that true end-diastolic and early systolic images could be acquired). The whole 400-millisecond cycle could be spanned, therefore, by using two RR intervals. By cycling the image plane location for the different time points, we obtained an image of each plane at every time point. To increase the time resolution to 20 milliseconds, this entire sequence was repeated three times with additional time delays of 20 milliseconds, ie, the timing of the stack of images was shifted by 20 milliseconds for each repeat.

Experimental Procedure

Ten mongrel dogs weighing 20 to 25 kg were anesthetized with pentobarbital (25 to 35 mg/kg) and fentanyl (5 mg/kg initial dose followed by 2 $mg \cdot kg^{-1} \cdot h^{-1}$), intubated, and ventilated. Animal care was in accordance with institutional guidelines. An atrial pacing electrode was introduced transvenously, and the pacing interval was kept constant at 400 milliseconds. Doppler echocardiography (Hewlett-Packard Sonos 1000) was used to determine the timing of end diastole, onset of ejection, end of ejection, and onset of filling. Tagged MR images were acquired throughout the cardiac cycle. Images acquired during periods of hemodynamic instability, defined as changes of >15% in mean arterial pressure, were rejected.

The heart was arrested in diastole with KCl, excised, and fixed with an intracoronary infusion of 4% buffered formaldehyde at a pressure of 100 mm Hg. The LV was cut along the exact short- and long-axis planes in which it was imaged. The proper planes in which to slice the pathological specimens were found by use of the distance to the mitral valve ring as a marker for identifying the imaged short-axis slices (equivalent to the long-axis tags) and use of the distance to the right ventricular insertions for identifying the imaged short-axis tags (equivalent to the long-axis slices). These distances (along the epicardial surfaces) were measured from the images in duplicate, ie, every short-axis tag was identified by its distance from both right ventricular insertions, and every long-axis tag was identified by its distance from both the ipsilateral and contralateral aspects of the mitral ring (the latter measured around the apex). The location of each epicardial tag intersection was thus determined on the pathological specimen and marked

with a pin, which then guided its sectioning into first short-axis slices and then individual blocks.

The blocks thus obtained, each corresponding to an imaged cuboid, were sectioned parallel to the epicardium. After the outermost 0.5 mm was discarded, the orientation of the fibers with respect to the short-axis plane was identified by use of a dissecting microscope. Similarly, fiber orientation was obtained halfway through the wall and 1 mm inward from the endocardial surface.

Data Analysis

Deformation at end ejection was quantified in this study by the normal and shear strains in a coordinate system aligned to the local fiber orientation of the LV epicardium and endocardium. These strains describe the shortening or lengthening along the perpendicular axes of this coordinate system and the shearing occurring in the planes described by two of the axes.

Strain Computations

Images were processed by a microcomputer-based dedicated contouring system (Dell 386). The point at which the midpoint of each tag intersected the epicardium and endocardium was identified visually and marked. This yielded *xy* coordinates of all tag intersections for each of the five short-axis and four long-axis images at each time point. Akima interpolation,[19] a method for generating smooth contours from a limited number of operator-selected points, was used to outline the epicardial and endocardial surfaces. Arc lengths between these tag points along the epicardial and endocardial surfaces were calculated. The long- and short-axis coordinates were then merged to obtain one unique set of *xyz* coordinates for each time point. This merging operation required interpolation between successive short-axis slices, since each short-axis slice was acquired in a fixed plane of space throughout the cardiac cycle, although the actual myocardium imaged at end diastole moved toward the apex during systole. The amount of this motion for each short-axis slice could be determined from the tagged long-axis images, since the tags on the long-axis images were placed at end diastole at planes identical to the short-axis image planes. Next, a translation of *xy* data was performed to a local coordinate system for each epicardial and endocardial node point (Fig 2). The new axes were radial (R), using the direction perpendicular to the wall (which is tilted near the apex because of the taper of the LV); circumferential (C), tangent to the surface and parallel to the short axis of the heart; and longitudinal (L), tangent to the surface and perpendicular to C. The coordinates for all node points were then expressed in this RCL coordinate system. Finally, using the histological fiber angle data, a rotation in the circumferential-longitudinal plane was performed to a coordinate system using the local fiber (F), cross-fiber (X), and radial (R) axes (Fig 2).

Displacements were then calculated for all epicardial and endocardial node points in this RFX coordinate system. From these displacements, normal strains were computed, ie, radial (thickening) strain, fiber strain, and cross-fiber strain. In addition, the fiber/cross-fiber shear strain was calculated.

Differential thickening of epicardium and endocardium, known to occur within the LV wall, was computed by defining a plane midway between the epicardial and endocardial surfaces at end diastole. This plane divided the cuboid into two elements with different volumes. Assuming constancy of volume of the myocardium, the ratio of the epicardial and endocardial volumes stays fixed throughout the cycle, so the coordinates of the midwall plane could be computed at any time point. This allows inner wall thickness changes to be considered separately from outer wall thickness changes. Midwall fiber shortening was calculated by interpolation of epicardial and endocardial circumferential and longitudinal strains using the location of the midwall plane, rotated into the measured midwall fiber orientation.

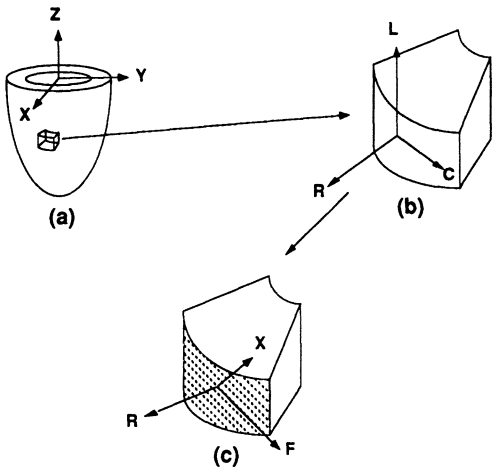

FIG 2. Diagrams showing coordinate systems for strain determination (see text). The long- and short-axis coordinates of the tag intersections with epicardium and endocardium measured in the external reference system of the magnet were merged to obtain one unique set of *xyz* coordinates (a). Next, a translation of *xyz* data is performed to a local coordinate system. The new axes are radial (R), using the direction perpendicular to the wall; circumferential (C), tangent to the surface and parallel to the short axis of the heart; and longitudinal (L), tangent to the surface and perpendicular to C (exploded cuboid in b). Finally, using the anatomic fiber angle data determined for each cuboid (indicated by the broken lines on the epicardial surface), a rotation in the circumferential-longitudinal plane around the R axis was performed to a coordinate system using the local fiber (F), cross-fiber (X), and radial (R) axes (c).

Assessing for Steady State During Experimental Protocols

Blood pressures before and after the entire sequence of images were compared. To further assess whether hemodynamic changes occurred during imaging, LV diameters were measured from the short-axis images (acquired at the start of the protocol) and from identical loci on the long-axis images (acquired at the end of the protocol) and compared.

Statistical Interpretation of Data

The entire data set, including 20 time points, was used for statistical analysis. Significant differences in strains were identified by repeated-measures ANOVA. The degree of inhomogeneity was analyzed by a two-factor ANOVA measuring regional heterogeneity of strain in the short axis (locations around the circumference of the ventricle) and long axis (levels from base to apex) of the ventricle.

Regional variations allowed statistical analysis of the relations between thickening and the various strains. Repeated-measures analyses of generalized linear models were performed by first extracting relations of strain to thickening across regions in each dog and then combining the resultant coefficient estimates across dogs. The relations of fiber strain variables to thickening were analyzed in both multiple and simple regression settings with and without accounting for the presence of other strains. A value of $P<.05$ was considered significant.

Results

Fiber Orientation

Average fiber angles with respect to the short-axis plane defined by pathological analysis were $-68.6\pm12.7°$, $10.5\pm3.6°$, and $74.5\pm4.2°$ for epicardium, midwall, and endocardium, respectively. Fig 3 shows fiber angles by region and level of the LV. Little

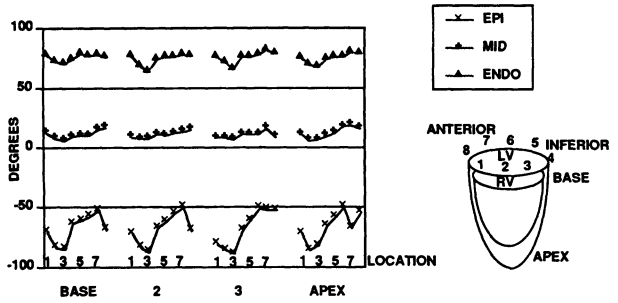

FIG 3. Plots and diagram showing fiber angles determined pathologically. Epicardial (EPI), midwall (MID), and endocardial (ENDO) fiber angles are plotted for each level of the left ventricle (LV) from base to apex. Angles are given with respect to the circumferential plane. Within each level, angles from eight individual locations representing the eight tagged segments around the short-axis circumference are plotted. These locations are defined in the diagram on the right. RV indicates right ventricle.

variability is present from base to apex. Around the circumference, however, fiber angles vary significantly, especially in the epicardium.

Hemodynamic Stability During Imaging

Blood pressure was 143±7/84±5 mm Hg before imaging and 139±8/82±6 mm Hg after imaging (P=NS). LV end-diastolic diameters at 20 loci from the short-axis images (four diameters from each of five short-axis slices) were compared with those from identical loci using the comparable long-axis images (five diameters from each of four long-axis images). The average time difference between the measurements was 65 minutes. The average diameter was 35.6±0.8 mm in the short axis and 35.7±0.7 in the long axis (mean±SEM, P=NS).

Strain Analysis

The results for the normal strains in the radial/fiber/cross-fiber coordinate system are shown in Fig 4. Thickening (radial strain, Fig 4, top) is the largest strain, averaging 32.5%. Most of this thickening occurs at the endocardial side of the wall (not shown in Fig 4), which shows almost twice the thickening of the epicardial side (43.3% versus 25.5%, $P<.001$). Strain in the fiber direction (fiber strain, Fig 4, middle) is similar at the epicardium and endocardium, −6.4% and −8.5%, respectively, $P>.05$. Midwall fiber strain, calculated from epicardial and endocardial strains, corresponds to 9.0%, which is not significantly different from epicardial and endocardial fiber strain. These results show that fiber shortening is homogeneous through the ventricular wall, as previously predicted by Arts et al[20] on the basis of computer models accounting for LV torsional deformation.

However, shortening perpendicular to the fibers in the plane parallel to the surface of the heart (cross-fiber, Fig 4, bottom) differs markedly between epicardium and endocardium. A very small strain, −0.6%, is observed at the epicardium, whereas at the endocardium the strain exceeds all other shortening strains, −25.1% (cross-fiber$_{endo}$>cross-fiber$_{epi}$, $P<.001$ and cross-fiber$_{endo}$>fiber$_{endo}$, $P<.001$). Therefore, at the endocardium, the deformation perpendicular to the fibers, in a direction in which no local active force generation takes place, is three times as large as the deformation in the direction of fiber orientation in which force is

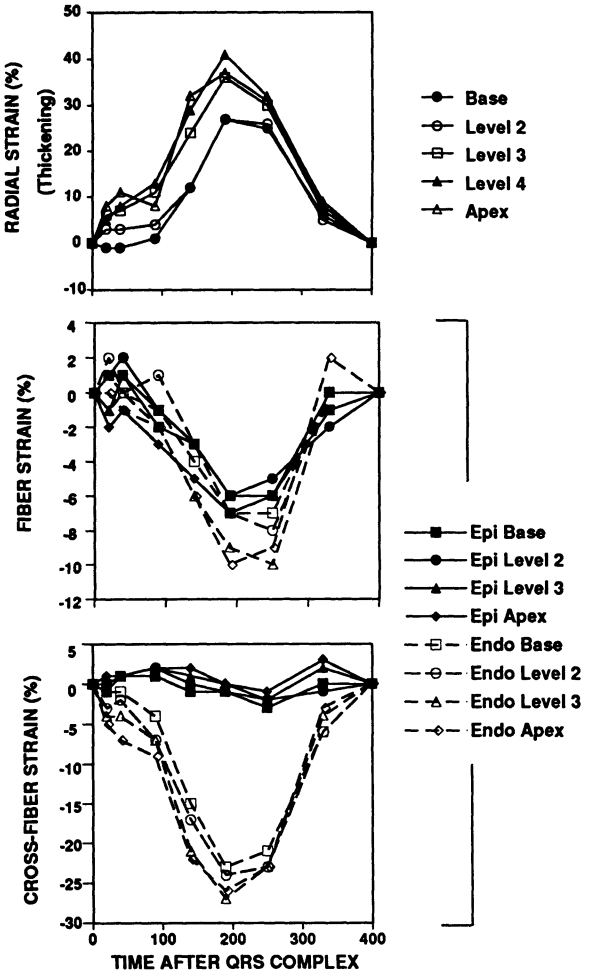

FIG 4. Graphs showing normal strains measured throughout the cardiac cycle at different short-axis levels of the ventricle from the base to the apex. Radial (thickening), fiber, and cross-fiber strains are shown. End systole (aortic valve closure) occurred at 190 milliseconds. Epi indicates epicardium; endo, endocardium.

generated. The inverse occurs at the epicardium, where fiber shortening is 10 times greater than the cross-fiber deformation.

The shear strain in the fiber/cross-fiber plane, which describes parallel sliding of fibers along their long axes, ie, displacement of fibers relative to each other along the fiber orientation, was small at epicardium and endocardium, 2.6% and 1.4%, respectively.

Regional Variations

Marked regional inhomogeneities are present in most strains. Although radial thickening is relatively constant around the circumference of the ventricle, a significant gradient exists from base to apex, with apical thickening exceeding basal thickening (40.3% versus 27.3%, $P<.001$, Fig 4, top, and Table 1). Shortening in the fiber direction shows a significant difference around the circumference of the ventricle (less epicardial shortening near insertions of the right ventricular free wall, Fig 5) but a more uniform base-to-apex behavior (Table 1). Regional differences for cross-fiber shortening are divergent for epicardium and endocardium; epicardial cross-fiber shortening is significantly different around the circumference of the ventricle but homogeneous from base to

TABLE 1. Left Ventricular Strains*

		Level				
	Mean±SD	**1**	**2**	**3**	**4**	***P***
Thickening	0.325±0.177	0.273±0.165	0.273±0.163	0.358±0.177	0.403±0.168	.0001
Fiber epi	−0.064±0.118	−0.061±0.097	−0.059±0.103	−0.063±0.155	−0.072±0.108	.917
Fiber endo	−0.085±0.100	−0.068±0.106	−0.075±0.088	−0.094±0.098	−0.105±0.107	.083
Cross-fiber epi	−0.006±0.082	−0.015±0.077	−0.008±0.074	−0.003±0.087	0.004±0.091	.511
Cross-fiber endo	−0.251±0.103	−0.225±0.093	−0.243±0.098	−0.271±0.107	−0.265±0.112	.022
Shear epi	0.026±0.093	0.02±0.077	0.019±0.083	0.035±0.094	0.029±0.116	.610
Shear endo	0.014±0.149	0.028±0.131	0.043±0.116	0.004±0.154	−0.022±0.187	.049

Epi indicates epicardium; endo, endocardium; and shear, fiber/cross-fiber shear. Values are mean±SD.
*Expressed first as average values, then broken down into levels of the left ventricle, from base (level 1) to apex (level 4), and locations around the circumference of the left ventricle (see Fig 3 for definitions). *P* values refer to the significance of the regional variations.

apex, whereas at the endocardium little difference is present around the ventricle but does exist along the long axis. Finally, shear in the fiber/cross-fiber plane is significantly different from base to apex at the endocardium and around the circumference of the ventricle, mainly at the right ventricular side of the septum.

Relation of Fiber Strains to Thickening

Six fiber strain variables (Table 2) were investigated to determine their relations to thickening in both multiple and simple regression settings, with and without accounting for the presence of other strains. In either setting, epicardial and endocardial cross-fiber strains were found to be important explanatory variables for total wall thickening ($P=.047$ and .001, respectively; Table 2). This underscores the relation between cross-fiber shortening and wall thickening.

In addition, investigation of the interrelations among these six fiber/strain variables showed strong correlations between fiber and cross-fiber strains of the opposite layers and complete absence of correlation within layers. Cross-fiber shortening at the endocardium was most closely related to fiber shortening at the epicardium ($P<.0001$), whereas cross-fiber shortening at the epicardium was closely related to endocardial fiber shortening ($P<.0001$). These results stress the strong interaction that exists between different layers of myocardium.

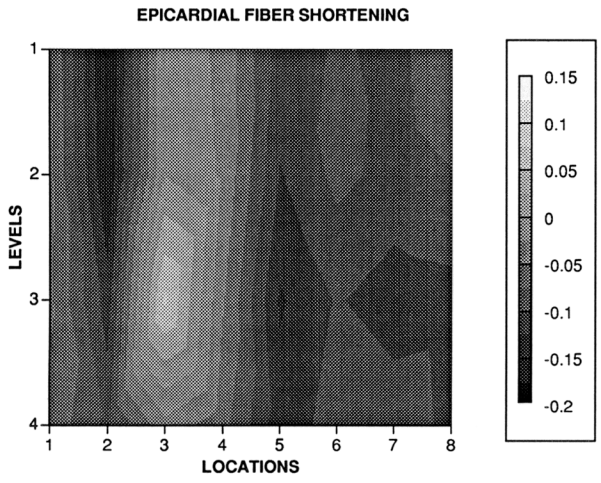

FIG 5. Contour map showing regional variation of epicardial fiber shortening. "Levels" refers to the base (level 1) to apex (level 4) direction. "Locations" refers to regions around the circumference of the left ventricle (see diagram in Fig 3). The darkest shading indicates the greatest shortening.

Discussion

In this study, the three-dimensional deformation of all regions of the LV with respect to the anatomically defined fiber orientation was quantified for the first time. A nondestructive technique that does not interfere with normal function of the myocardium was used. Fiber strain is approximately −8% and is not significantly different at epicardial, midwall, or endocardial layers. The deformation perpendicular to the fiber orientation in the plane of the fibers is small at the epicardium and increases toward the endocardium, where it exceeds fiber shortening by threefold (about −25%). Thickening is the largest strain (about 32%).

Although a single fiber or papillary muscle preparation contracting against a load will shorten in one direction and lengthen or thicken in the other two perpendicular directions, this study shows that in the intact heart, in one of these perpendicular directions, shortening rather than lengthening occurs. At the endocardium, this cross-fiber shortening far exceeds fiber shortening. Since active shortening of any layer can occur only in the direction in which the sarcomeres are aligned, this phenomenon must be explained by a force acting from a distance. The likely candidates for generation of this force are fibers in other layers that have at least a component of shortening in the perpendicular or cross-fiber direction (Fig 6). Since the fiber angle changes extensively through the wall (Fig 3), a perpendicular component exists somewhere in the wall for all layers. The strong correlation between fiber strains on one side of the wall with cross-fiber strains on the other, shown in this study (Table 2), strongly suggests that this force is transmitted through the wall.

Most cross-fiber shortening occurs at the endocardium, likely driven by the perpendicular components of fibers residing in the more epicardial layers. Epicardium therefore affects endocardium more than vice versa. This may be because the epicardial muscle mass is greater than that of the endocardium, because its surface area is larger, owing to the difference in radius. Also, geometric factors are likely to play a role in normal hearts: the curvature of epicardium and en-

TABLE 1. Continued

Location								
1	2	3	4	5	6	7	8	*P*
0.299±0.154	0.325±0.195	0.353±0.149	0.326±0.202	0.284±0.144	0.370±0.214	0.314±0.170	0.327±0.173	.418
−0.025±0.080	−0.112±0.099	0.022±0.213	−0.026±0.094	−0.105±0.092	−0.085±0.068	−0.094±0.084	−0.084±0.081	.0001
−0.126±0.122	−0.053±0.085	−0.099±0.071	−0.105±0.109	−0.063±0.076	−0.058±0.116	−0.081±0.097	−0.097±0.098	.011
−0.003±0.085	0.041±0.061	0.030±0.085	−0.041±0.089	0.002±0.083	−0.013±0.051	−0.032±0.070	−0.029±0.092	.0001
−0.247±0.088	−0.245±0.083	−0.221±0.108	−0.241±0.113	−0.244±0.106	−0.282±0.086	−0.281±0.089	−0.244±0.138	.152
0.077±0.099	0.002±0.080	0.081±0.088	0.071±0.078	−0.032±0.088	−0.017±0.081	−0.006±0.075	0.029±0.077	.0001
0.054±0.148	−0.013±0.109	0.039±0.105	0.005±0.180	−0.005±0.122	0.038±0.136	−0.004±0.200	−0.000±0.166	.355

docardium is convex toward the cavity. In an arched structure the outer fibers display a larger torque than the inner ones for the same amount of shortening. This translates into a dominance of epicardium over endocardium and extensive cross-fiber shortening at the endocardium. The interaction, however, is bidirectional, as demonstrated by the (smaller) cross-fiber shortening also present at the epicardium.

How the deformation in the cross-fiber direction is organized at the cellular level remains to be determined. Spotnitz et al[21] and Waldman et al[9] suggested that fibers must be either rearranged or flattened to account for the observed changes in dimension. The difference between these two possibilities reflects only the anatomic level at which structural rearrangement takes place. If the deformation is present at the level of the fibers themselves, they could become flattened in one direction and bulge in the other direction and the myofibrils within them would be rearranged. If the deformation is at the level of the fiber bundles, each bundle would form a more oval cross section and the fibers within them would be rearranged with respect to each other. Data obtained by Spotnitz et al[21] in rat hearts fixed at high volumes (diastolic) and low volumes (systolic) showed a larger number of fibers across the wall thickness in the systolic hearts, supporting the contention that deformational changes occur at the level of the fiber bundles. Those authors suggested that rearrangement might occur along open spaces or sliding planes between groups of muscle fibers.

Cross-fiber shortening could simply represent the convergence of loose endocardial trabecular tissue. However, this appears unlikely, since cross-fiber shortening occurs in the epicardium, where trabeculation is completely absent, as well as in the endocardium (although to a smaller extent); its presence was previously noted in studies of bead deformation,[8,9] in which the beads were later verified to have been implanted in packed myocardial tissue; and its direction is oblique (as is the direction of endocardial principal strain[9,13]), whereas trabeculae run along the long axis of the LV.

Waldman et al,[9] using implanted radiopaque beads, previously studied fiber and cross-fiber strains in the anterior free wall of the canine LV. They reported fiber strain values very close to ours. Cross-fiber strains were also similar, although slightly lower in the endocardium (−0.17 compared with our −0.24). The differences can be explained by the depth at which the measurements were obtained (22% and 65% through the wall in Waldman's study and 10% and 90% in this study, taking pixel size of the MR images into account), by the differences between open- and closed-chest preparations, and by the possibility that the results using the radiopaque markers are slightly altered by injury of the myocardium. The general trend, ie, similar fiber shortening at epicardium and endocardium and cross-fiber shortening being smaller than fiber shortening at the epicardium and larger at the endocardium, is consistent. The relation of fiber and cross-fiber strains to thickening

TABLE 2. Results of the Univariate Repeated-Measures Regression Analysis

	Dependent Variables								
	Total Thickening			Epi Cross-Fiber Shortening			Endo Cross-Fiber Shortening		
Independent Variables	Mean	SEM	*P*	Mean	SEM	*P*	Mean	SEM	*P*
Fiber epi	0.04	0.08	.63	−0.03	0.08	.74	0.33	0.04	<.0001
Fiber endo	−0.06	0.05	.26	0.63	0.07	<.0001	−0.0006	0.04	.99
Cross-fiber epi	0.16	0.07	.047				0.38	0.08	.001
Cross-fiber endo	−0.32	0.07	.001	0.38	0.08	.001			
Shear epi	0.04	0.05	.45	−0.01	0.03	.68	0.19	0.04	.001
Shear endo	0.04	0.06	.46	−0.09	0.03	.015	−0.02	0.05	.68

Epi indicates epicardial; endo, endocardial. Total thickening and cross-fiber shortening are dependent variables; all fiber strains are independent variables.

Values of $P<.05$ are considered significant.

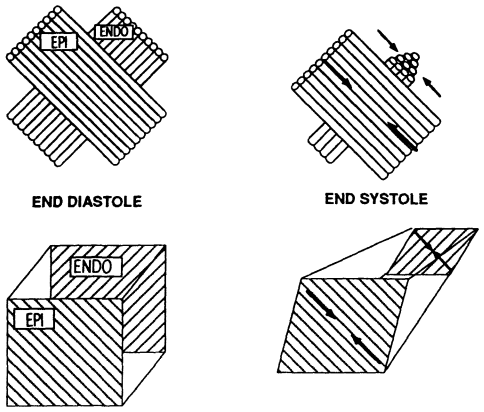

FIG 6. Top, Diagrams of fibers in the subepicardium (EPI) and subendocardium (ENDO), oriented approximately at right angles to each other. The diagrams depict how shortening of epicardial fibers (arrows) might cause endocardial cross-fiber shortening and fiber rearrangement. Bottom, Depiction of "cubes" of myocardium, illustrating how this endocardial deformation in the cross-fiber direction may lead to extensive thickening. Hatching indicates fiber direction. Note that although fiber angles at the epicardial and endocardial surfaces were separated by only 37° in this study, fibers located deeper within the walls are closer to perpendicular.

was not studied, since only one region was available per dog.

The strong relation between wall thickening and cross-fiber strains found in the regression analyses supports the hypothesis that transmission of force from layer to layer through the wall, resulting in cross-fiber shortening, is an important mechanism for extensive wall thickening, although further experiments are needed to prove the causal relation. The interaction between layers of the heart wall may occur through connective tissue attachments; fibers are embedded in a woven network of collagen that would allow contractile forces to be distributed through the wall.[22] Nevertheless, components of the network are elastic and might allow stretching in the radial direction, required for fiber rearrangement. For example, the coiled perimysial collagen fibers may become uncoiled by systolic rearrangement at the fiber bundle level.[23] This stretching could be the basis for the buildup of restoring forces, which are released in early diastole to aid in early LV filling.[24-27] Finally, the straight collagen struts along the long axis of fibers and fiber bundles are likely to restrain sliding of these elements; this is supported by the small amount of fiber/cross-fiber shear strain (<3%) that would correspond to such sliding. Alternatively, the interaction between layers of the ventricular wall may be largely geometrical, through the shape constraints imposed by a thick-walled ellipsoid. In either case, this interaction appears to be a major contributor to extensive thickening and is thus an integral part of efficient ejection.

Potential Limitations

Resolution of MR Tag Displacement

The line resolution of the MRI system has been measured experimentally in phantoms by determination of the smallest change in tag separation that can be reproducibly detected with the imaging parameters described above. This resolution varies depending on the component of the tag separation in the frequency and phase directions but averages 0.57 mm. In a model of a moving phantom undergoing displacements of known magnitudes in three dimensions, the average error in the measurement of tag displacement was found to be 0.34 ± 0.12 mm.[13] These values are satisfactory for measuring strains of physiological magnitudes.

Homogeneity Within Each Cuboid

Since regional variation of strains in planes parallel to the epicardial and endocardial surfaces was demonstrated, the question arises whether there is adequate homogeneity between each pair of adjacent tags to calculate meaningful strains with these methods. The average segment lengths of the epicardial arc, endocardial arc, long-axis edge, and wall thickness in this study were 1.92, 1.32, 1.05, and 0.78 cm, respectively. Positioning the tags closer together would have reduced the amount of tag displacement during systole and approached the limits of our image resolution. Note that beads[8,9,11] or other devices[10,14,28] implanted for strain analysis in previous studies have usually been separated by at least 1 to 2 cm. Therefore, previous invasive studies of strain have assumed homogeneity over similar or greater distances.

Possible Fiber Angle Changes During Systole

In this study, fiber directions from arrested hearts were used to derive fiber and cross-fiber strains. If large changes in fiber angle occurred during the cardiac cycle, an error would be introduced. However, Streeter and Hanna[29] reported only insignificant differences of 0° to 4° in fiber pitch between distended ("diastolic") and contracted ("systolic") arrested hearts. The error induced by applying fiber angles measured in a "diastolic" arrested heart to strains that occur during the cycle should therefore be small.

Shrinkage During Fixation

Shrinkage during tissue processing could distort both fiber angle determination and identification of the midwall plane if it were not uniform. However, very little shrinkage of the dog heart occurred during Formalin fixation—the mass of nonbeating LVs was measured by MRI before and after fixation, and it changed <4% in all dogs. Significant shrinkage does occur during embedding of tissue blocks, but that potential error was avoided in this study by determination of the fiber angles from the gross specimen without embedding, by use of a dissecting microscope.

Maintenance of a Steady State During Experimental Protocols

Although a single MR image can be obtained in 3 minutes, it took about 2 hours to derive the full set of images with 20-millisecond time resolution. Changes in heart size or function during this time period would render the three-dimensional reconstruction inaccurate. However, it should be emphasized that this study used a closed-chest preparation with a minimum of instrumentation, which is not nearly as susceptible to instability as open-chest models. Maintaining a steady state over that time period did not present a difficulty for most of these dogs. Both blood pressure and LV

diameters were shown to be unchanged before and after imaging. Constancy of heart rate was obtained by pacing. Those dogs that did show hemodynamic instability, defined as sustained changes of >15% in mean arterial pressure that could not be corrected by adjustment of the anesthesia or fluid administration, were rejected from the analysis. There were 3 such dogs in addition to the 10 studied. It is therefore very unlikely that hemodynamic changes influenced our results.

Phasic Cuboid Volume Changes Over the Cardiac Cycle

Myocardial blood content may fall as intramural tension increases, so some systolic shortening could conceivably be attributed to loss of overall volume during the cycle. Also, if these changes are different in the epicardium and endocardium, our conclusions with respect to midwall shortening and inner and outer half thickening would be altered. However, we believe that these effects are small and do not seriously impact our conclusions, because most estimates suggest that blood accounts for only a small proportion of myocardial volume. Indeed, we have been unable to show a significant change in cuboid volume from end diastole to end systole; for the group of 10 dogs reported here, the mean cuboid volumes (±SEM) at end diastole, mid ejection, end ejection, and mitral valve opening were 1.67±0.03, 1.71±0.03, 1.86±0.04, and 1.78±0.03 cm^3, respectively (P=NS). This is consistent with previous studies of myocardial volume through the cycle, which also did not show a significant decrease during systole.[30]

Implications

Our results strongly support the hypothesis that although some thickening can occur by simple shortening of fibers acting individually, extensive wall thickening can exist only through the interaction of layers and a structural rearrangement of fibers, made possible by the intricate fiber organization of the LV wall. Whereas this structure probably maintains similar stresses at the fiber level as evidenced by the constant fiber strains throughout the wall, the interaction between layers directs the maximal deformation toward radial thickening at the endocardium, combining the action of all layers toward the efficient ejection of blood. Because thickening at the endocardium far exceeds that at the epicardium,[31] the endocardial myocardium is often considered the working half of the wall, whereas the epicardial myocardium is thought merely to limit eccentric movement of the more internal layers. The quantification of strains and their interaction shown in this study attribute a far more important role to the epicardial layers in overall performance of the ventricle than is usually assumed.

Disease processes that alter interactions between layers of the heart wall will therefore profoundly influence pump function. Disorders of the connective tissue matrix that have been documented in hypertrophic heart disease and some forms of cardiomyopathy[21,32-39] might affect cardiac performance in this way. In addition, cardiac remodeling caused by ischemia, infarction, or volume overload could modify thickening by changing the relative fiber angles across the wall. Three-dimensional MRI analysis would be an excellent technique for defining mechanisms of dysfunction and effects of interventions in these disease states.

Acknowledgments

This study was supported in part by National Heart, Lung, and Blood Institute (NHLBI) Ischemic Heart Disease SCOR grant HL-1765516, NHLBI grant RO1-HL-46223 (E.P.S.), and NHLBI grant RO1-HL-43722 (J.L.W.). F.E.R. is a research fellow at the Johns Hopkins University supported by a NATO fellowship. We are grateful for the excellent technical assistance of Stephanie Bosley and the skilled computing assistance of Susan Benac.

References

1. Eisenberg E, Hill JL. Muscle contraction and free energy transduction in biological systems. *Science.* 1985;277:999-1004.
2. Sonnenblick EH, Ross J Jr, Covell JW, Spotnitz HM, Spiro D. The ultrastructure of the heart in systole and diastole. *Circ Res.* 1967; 21:423-431.
3. Abboth BC, Mommaerts WFHMA. A study of inotropic mechanisms in the papillary muscle preparation. *J Gen Physiol.* 1959;42: 533-541.
4. Streeter DD Jr, Spotnitz HM, Patel DP, Ross J Jr, Sonnenblick EH. Fiber orientation in the canine left ventricle during diastole and systole. *Circ Res.* 1969;24:339-347.
5. Carew TE, Covell JW. Fiber orientation in hypertrophied canine left ventricle. *Am J Physiol.* 1979;236:H487-H493.
6. Greenbaum RA, Ho SY, Gibson DG, Becker AE, Anderson RH. Left ventricular fibre architecture in man. *Br Heart J.* 1981;45: 248-263.
7. Sallin EA. Fiber orientation and ejection fraction in the human left ventricle. *Biophys J.* 1969;9:954-964.
8. Waldman LK, Fung YC, Covell JW. Transmural myocardial deformation in the canine left ventricle: normal in vivo three-dimensional finite strains. *Circ Res.* 1985;57:152-163.
9. Waldman LK, Nosan D, Villarreal F, Covell JW. Relation between transmural deformation and local myofiber direction in canine left ventricle. *Circ Res.* 1988;63:550-562.
10. Prinzen FW, Arts T, Hoeks APG, Reneman RS. Discrepancies between myocardial blood flow and fiber shortening in the ischemic border zone as assessed with video mapping of epicardial deformation. *Pflugers Arch.* 1989;415:220-229.
11. Ingels NB Jr, Hansen DE, Daughters GT, Stinson EB, Alderman EL, Miller DC. Relation between longitudinal, circumferential, and oblique shortening and torsional deformation in the left ventricle of the transplanted human heart. *Circ Res.* 1989;64:915-927.
12. Ingels NB Jr, Daughters GT, Stinson EB, Alderman EL, Miller DC. Three-dimensional left ventricular midwall dynamics in the transplanted human heart. *Circulation.* 1990;81:1837-1848.
13. Azhari H, Weiss JL, Rogers WJ, Siu CO, Zerhouni EA, Shapiro EP. Noninvasive quantification of principal strains in normal canine hearts using tagged MRI images in 3-D. *Am J Physiol.* 1993;264(*Heart Circ Physiol* 33):H205-H216.
14. Villarreal FJ, Lew WYW. Finite strains in anterior and posterior wall of the canine left ventricle. *Am J Physiol.* 1990;259(*Heart Circ Physiol* 28):H1409-H1418.
15. Douglas AS, Hunter WC, Wiseman MD. Inhomogeneous deformation as a source of error in strain measurements derived from implanted markers in the canine left ventricle. *J Biomech.* 1990;23: 331-341.
16. Zerhouni EA, Parish DM, Rogers WJ, Yang A, Shapiro EP. Human heart: tagging with MR imaging: a method for noninvasive assessment of myocardial motion. *Radiology.* 1988;169:59-63.
17. Buchalter MB, Weiss JL, Rogers WJ, Zerhouni EA, Weisfeldt ML, Beyar R, Shapiro EP. Noninvasive quantification of left ventricular rotational deformation in normal humans using magnetic resonance imaging myocardial tagging. *Circulation.* 1990;81: 1236-1244.
18. McVeigh ER, Zerhouni EA. Noninvasive measurement of transmural gradients in myocardial strain with MR imaging. *Radiology.* 1991;180:677-683.
19. Akima H. A new method of interpolation and smooth curve fitting based on local procedures. *J Assoc Comp Mach.* 1970;17:589-602.
20. Arts T, Meerbaum S, Reneman RS, Corday E. Torsion of the left ventricle during the ejection phase in the intact dog. *Cardiovasc Res.* 1984;18:183-193.
21. Spotnitz HM, Spotnitz WD, Cottrell TS, Spiro D, Sonnenblick EH. Cellular basis for volume related wall thickness changes in the rat left ventricle. *J Mol Cell Cardiol.* 1974;6:317-331.
22. Ohayon J, Chadwick RS. Effects of collagen microstructure on the mechanics of the left ventricle. *Biophys J.* 1988;54:1077-1088.

23. Robinson TF, Geraci MA, Sonnenblick EH, Factor SM. Coiled perimysial fibers of papillary muscle in rat heart: morphology, distribution, and changes in configuration. *Circ Res.* 1988;63: 577-592.
24. Robinson TF, Factor SM, Sonnenblick EH. The heart as a suction pump. *Sci Am.* 1986;254:84-91.
25. Park CH, Chow WH, Gibson DG. Phase differences between left ventricular wall motion and transmitral flow in man: evidence for involvement of ventricular restoring forces in normal rapid filling. *Int J Cardiol.* 1989;24:347-354.
26. Udelson JE, Bacharach SL, Cannon RO III, Bonow RO. Minimum left ventricular pressure during β-adrenergic stimulation in human subjects: evidence for elastic recoil and diastolic "suction" in the normal heart. *Circulation.* 1990;82:1174-1182.
27. Covell JW. Factors influencing diastolic function: possible role of the extracellular matrix. *Circulation.* 1990;81(suppl III):III-155-III-158.
28. Arts T, Veenstra PC, Reneman RS. Epicardial deformation and left ventricular wall mechanics during ejection in the dog. *Am J Physiol.* 1982;243:H379-H390.
29. Streeter DD Jr, Hanna WT. Engineering mechanics for successive states in canine left ventricular myocardium. *Circ Res.* 1973;33: 654-656.
30. Iwasaki T, Sinak JL, Hoffman EA, Robb RA, Harris LD, Bahn RC, Ritman EL. Mass of left ventricle myocardium estimated with the dynamic spatial reconstructor. *Am J Physiol.* 1984;246: H138-H142.
31. Gallagher KP, Osakada G, Matsuzaki M, Miller M, Kemper WS, Ross J Jr. Nonuniformity of inner and outer systolic wall thickening in conscious dogs. *Am J Physiol.* 1985;249:H241-H248.
32. Abrahams C, Janicki JS, Weber KT. Myocardial hypertrophy in *Macaca fascicularis:* structural remodeling of the collagen matrix. *Lab Invest.* 1987;56:676-683.
33. Weber KT, Pick R, Janicki JS, Gadodia G, Lakier JB. Inadequate collagen tethers in dilated cardiopathy. *Am Heart J.* 1988;116: 1641-1646.
34. Capasso JM, Robinson TF, Anversa P. Alterations in collagen cross-linking impair myocardial contractility in the mouse heart. *Circ Res.* 1989;65:1657-1664.
35. Weber KT. Cardiac interstitium in health and disease: the fibrillar collagen network. *J Am Coll Cardiol.* 1989;13:1637-1652.
36. Weber KT, Pick R, Silver MA, Moe GW, Janicki JS, Zucker IH, Armstrong PW. Fibrillar collagen and remodeling of dilated canine left ventricle. *Circulation.* 1990;82:1387-1401.
37. Brilla CG, Pick R, Tan LB, Janicki JS, Weber KT. Remodeling of the rat right and left ventricles in experimental hypertension. *Circ Res.* 1990;67:1355-1364.
38. Yun KL, Niczyporuk MA, Daughters GT II, Ingels NBJ, Stinson EB, Alderman EL, Hansen DE, Miller DC. Alterations in left ventricular diastolic twist mechanics during acute human cardiac allograft rejection. *Circulation.* 1991;83:962-973.
39. Weber KT, Brilla CG. Pathological hypertrophy and cardiac interstitium: fibrosis and renin-angiotensin-aldosterone system. *Circulation.* 1991;83:1849-1865.